*R*esearch in
*A*stronomy and
*A*strophysics

A multiwavelength study of the star forming H II region Sh2-82

Nai-Ping Yu[1,2], Jun-Jie Wang[1,2]

[1] National Astronomical Observatories, Chinese Academy of Sciences, Beijing 100012, China;
   yunaiping09@mails.gucas.ac.cn
[2] NAOC-TU Joint Center for Astrophysics, Lhasa 850000, China

Abstract Based on a multiwavelength study, the interstellar medium and young stellar objects (YSOs) around the H II region Sh2-82 have been analyzed. Two molecular clumps were found from the archival data of the Galactic Ring Survey, and using the Two Micron All-Sky Survey catalog, we found two corresponding young clusters embedded in the molecular clumps. The very good relations between CO emission, infrared shells and YSOs suggest that it is probably a triggered star formation region from the expansion of Sh2-82. We further used the data from the Galactic Legacy Infrared Mid-Plane Survey Extraordinaire from *Spitzer* to study the YSOs within the two clumps, confirming star formation in this region. By spectral energy distribution fits to each YSO candidate with infrared excess, we derived the slope of the initial mass function. Finally, comparing the H II region's dynamical age and the fragmentation time of the molecular shell, we discard the "collect and collapse" process as being the triggering mechanism for YSO formation. Sh2-82 can be a mixture of other processes such as radiative-driven implosion and/or collisions with pre-existing clumps.

Key words: ISM: clouds — nebulae: H II region — individual: Sh2-82 — stars: formation

1 INTRODUCTION

Given that our own solar system probably formed in a massive cluster (Hester et al. 2004), knowledge of triggered star formation is necessary for understanding our own formation. Massive stars can strongly influence their surrounding environment via stellar winds, ionizing radiation and the expansion of H II regions. Since Elmegreen & Lada (1977) presented a mechanism for the sequential star formation of OB subgroups in molecular clouds, a number of mechanisms by which massive stars can affect the subsequent star formation around H II regions have been proposed. Two of the most studied mechanisms for triggering star formation in H II regions are "radiatively driven implosion" (RDI) (e.g. Lefloch & Lazareff 1994; Miao et al. 2006; Miao et al. 2009) and "collect and collapse" (C&C) (Elmegreen & Lada 1977). In the RDI model, pre-existing molecular clumps in the cloud become surrounded on all sides by high-pressure ionized gas heated by UV radiation, leading to the formation of a cometary globule (Bertoldi & McKee 1990). A dense core will form in the cometary globule where star formation will finally take place. In the C&C model, a slow-moving D-type ionization front has an associated shock front that precedes the ionization front. Dense gas may pile up between the two fronts. Over a long time, the compressed shocked layer becomes gravitationally unstable and fragments into dense clumps.
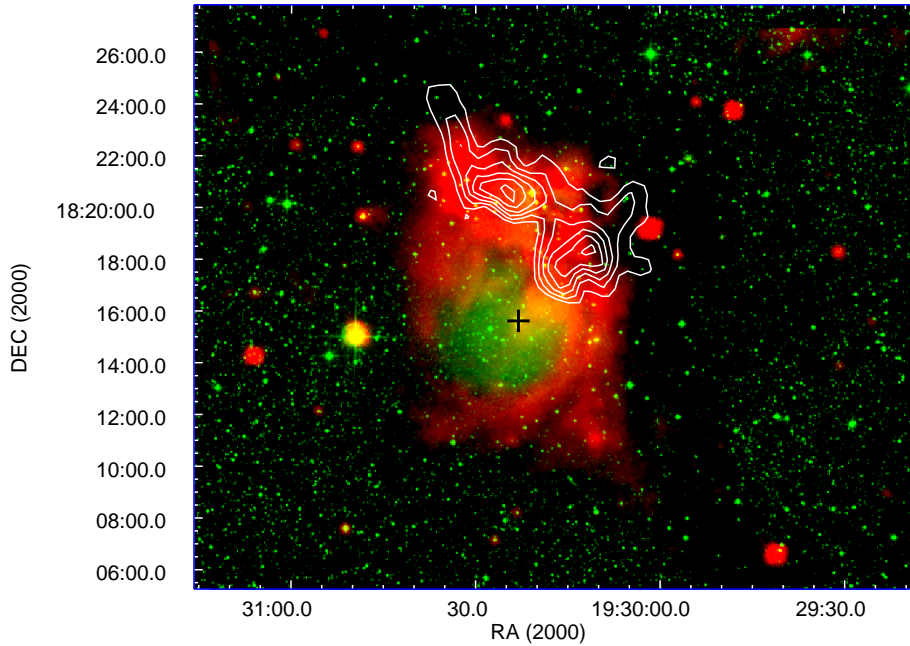
Fig. 1 Integrated emission of ^{13}CO (1–0) between 20.5 km s^{-1} and 27.5 km s^{-1} superimposed on the DSS (*green*) and MSX A band (*red*) pictures. The contour levels are from 8 K km s^{-1} to 18 K km s^{-1} in steps of 2 K km s^{-1}. The black cross represents the ionizing star HD 231616.

With the aim of increasing the observational evidence of triggered star formation in the surroundings of H II regions, we present a multiwavelength study of the molecular environment and young stellar objects (YSOs) of the H II region Sh2-82. Sh2-82 is ionized by HD 231616, a B0V/III star with a mass of 18 $M_\odot$ (Hunter & Massey 1990) (Fig. 1). The distance of Sh2-82 can be estimated in several ways. Based on $UBVRI$ photoelectric photometry, Lahulla (1985) derived a mean distance of 1.58 kpc, with the data ranging from 1.40 kpc to 1.80 kpc. From simulated B and V photometry formed through IIDS spectra of star(s), Hunter & Massey (1990) derived the distance of the ionizing star in Sh2-82 to be 1.7 kpc. According to the galactic rotation model of Brand & Blitz (1993) (with $R_\odot$=8.2 kpc and $v_\odot = 220$ km s^{-1}), we obtain a kinematic distance of either 2.1 kpc or 8.5 kpc. This ambiguity arises because we are studying a region in the first galactic quadrant, where a given velocity may be associated with two possible distances. Considering that distances derived by photometry are more accurate than the other two methods, we use a distance of 1.8 ± 0.4 kpc for Sh2-82 in the following discussion.

2 DATA SETS, REDUCTIONS AND RESULTS

2.1 Galactic Ring Survey

We analyzed the radio emission of ^{13}CO (1–0) in the region of Sh2-82 using the Galactic Ring Survey (GRS; Jackson et al. 2006). The survey used the SEQUOIA multi pixel array on the Five College Radio Astronomy Observatory's 14 m telescope to cover a longitude range of $\ell = 18°{\sim}55.7°$ and a latitude range of $|b| < 1°$, fully sampled with a pixel size of 22 arcsec from 1998 to 2005. The survey's velocity coverage is -5 to 135 km s^{-1} for galactic longitudes $\ell \leq 40°$ and -5 to 85 km s^{-1}
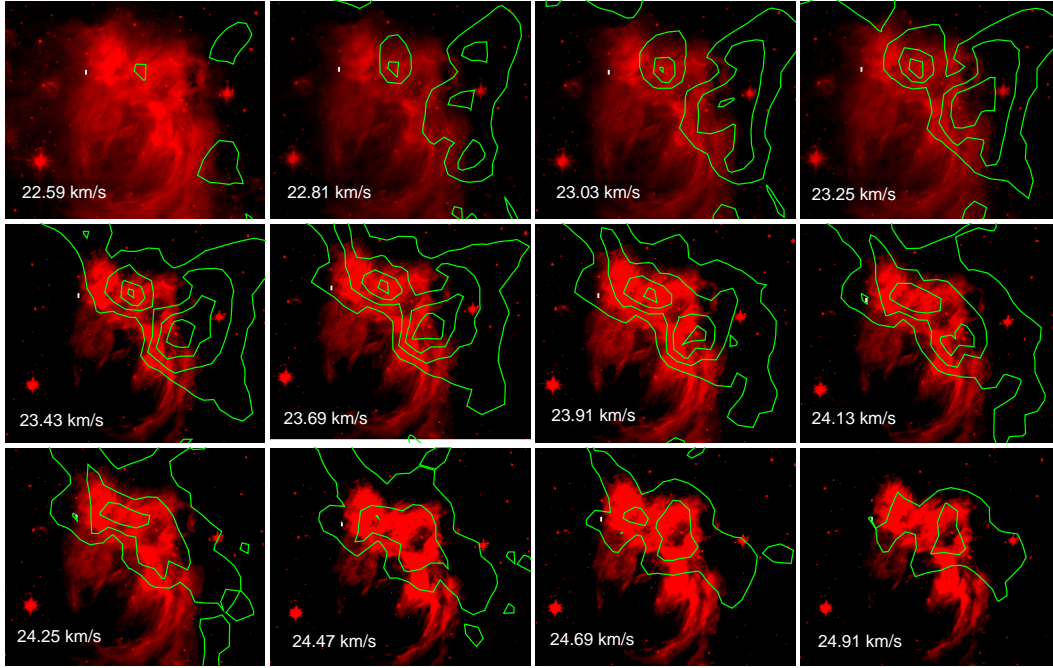
Fig. 2 Channel maps of the ^{13}CO (1–0) emission every 0.22 km s^{-1} superimposed on the Spitzer 8.0 μm image. The green contour levels are 2, 4, 6 and 8 K km s^{-1}.

for galactic longitudes $\ell > 40°$. The spectral resolution for both velocity ranges is 0.21 km s^{-1}. The data cube was reduced with IDL procedures.

Figure 1 shows a distinctive ring morphology in the MSX A band detection. The 8.3 μm emission is dominated by intense line emission from polycyclic aromatic hydrocarbons (PAHs), arising at the interface between ionized gas in the H II region and the surrounding molecular material. We inspected the molecular gas around Sh2-82 from the GRS data in the whole velocity range and found an interesting feature around $\upsilon \sim 24$ km s^{-1} (Fig. 2). Two molecular clumps are evident on the northern photo dominated region (PDR) bordering Sh2-82. The very good correspondence between the H II region border traced by the IR emission and the molecular gas strongly suggests that the observed molecular gas is associated with Sh2-82. We used the central velocity of the molecular gas to infer its kinematic distance.

Using the ^{13}CO (1–0) line and under the assumption of local thermodynamic equilibrium (LTE), the H$_2$ column density and the masses of the two clumps can be estimated. We use

$$N(^{13}\mathrm{CO}) = 2.4 \times 10^{14} \frac{T_{\mathrm{ex}} \int \tau_{13} d\upsilon}{1 - \exp(-5.29/T_{\mathrm{ex}})} \tag{1}$$

to obtain the column density, where τ_{13} is the optical depth. We assume that the ^{13}CO emission is optically thin, the excitation temperature $T_{\mathrm{ex}} = 20$ K and the solar abundance ratios [H$_2$]/ [^{12}CO] $=10^4$ and [CO]/[^{13}CO]$= 89$ (Wilson & Rood 1994). The molecular masses were obtained from

$$M[M_\odot] = 4.2 \times 10^{-20} N(H_2) D^2 A, \tag{2}$$

where D is the distance in pc and A is the solid angle in steradians. The masses we derived were 2400 $M_\odot$ and 8600 $M_\odot$, respectively, for the two clumps.

2.2 2MASS Point Sources

We searched the environment of Sh2-82 for IR star clusters to locate sites of recent star formation. Based on a sample of YSOs having low and intermediate masses, Kerton et al. (2008) inferred color criteria to analyze the presence of star formation activity in the surroundings of the H II region KR 140. Kerton et al. (2008) divided their YSO candidates into four groups (P_1, P_{1+}, P_2, P_3) according to different photometric qualities and the adopted color criteria. P_1 sources have valid photometry in all three bands (i.e. ph qual values = A, B, C or D). The color criteria are $(J - H) > 1$ and $(J - H) - 1.7(H - K) + 0.075 < 0$. This approach selects stars lying below the reddening vector associated with an O6V star. P_{1+} sources also have valid photometry in all three bands. The color criteria are $1.3 < (J - H) < 1.6$, $(J - H) - 1.7(H - K) + 0.075 > 0$, $(J - H) - 1.7(H - K) - 0.3805 < 0$ and $K > 14.5$. This method selects YSOs lying in the overlapping region of T Tauri and main sequence stars. The P_2 group has not been detected in the J band. Thus the actual position of P_2 sources in the $(J - H)$ axes should be towards higher values. The P_2 color criteria are $(J - H) - 1.7(H - K) + 0.075 < 0$ and $(H - K) > 1.0$. Sources belonging to the P_3 group have J and H magnitudes that are lower limits, so their color $(J - H)$ cannot be determined. The P_3 color criterion is $(H - K) > 1.0$. Following such criteria, we searched for tracers of stellar formation activity in the 2MASS catalog, finding two YSO clusters associated with each molecular clump (Fig. 4).

Figure 3 shows the color-color diagram for the YSO candidates. The two parallel lines are reddening vectors, assuming the interstellar reddening law of Rieke & Lebofsky (1985) (A_J / A_V = 0.282; A_H / A_V = 0. 175; A_K / A_V = 0.112). Figure 4 shows the two young clusters embedded in the two molecular clumps.

2.3 Spitzer Data

The Galactic Legacy Infrared Mid-Plane Survey Extraordinaire (GLIMPSE I; Benjamin et al. 2003) covered the galactic plane ($10° < |\ell| < 65°$, $|b| < 1°$) with the four mid-IR bands (3.6, 4.5, 5.8, 8.0 μm) of the Infrared Array Camera (IRAC; Fazio et al. 2004) on the Spitzer Space Telescope. IRAC has a resolution of $1.5'' – 1.9''$ (3.6–8.0 μm). In this region we used the highly reliable GLIMPSE I Catalog with the sources detected in four bands (The highly reliable GLIMPSE I, II and 3D catalogs consist of point sources that are detected at least twice in one band with S/N > 5, and at least once in an adjacent band). The GLIMPSE I Catalog also tabulates JHK_S flux densities from the 2MASS point source catalogs (Skrutskie et al. 2006) for all GLIMPSE sources with 2MASS identifications.

MIPSGAL (Carey et al. 2005) is a legacy program covering the inner galactic plane $10° < |\ell| < 65°$ and $|b| < 1°$ at 24 and 70 μm with the Multiband Imaging Photometer on Spitzer (MIPS; Rieke et al. 2004). It has a resolution of $6''$ at 24 μm and $18''$ at 70 μm. MIPSGAL point-source catalogs were not yet available at the time of this study. For the 24 μm band, we used the APEX 1-Frame routines and the point response function (PRF) provided on the Spitzer Science Center's website to perform point-source PRF-fitting photometry. If an archive source was located within $2.4''$ of a 24 μm source, it was considered to have a 24 μm detection. For sources that APEX failed to detect automatically, we used the user list option in APEX to supply the coordinates for these sources to successfully derive a PSF fit.

With highly reliable infrared detections, we can distinguish YSOs from normal stars, i.e. main-sequence, giant and supergiant stars, from their excess IR emission, as they are enshrouded in dust that absorbs stellar UV and optical radiation. The regions in the left image of Figure 5 indicate stellar evolutionary stages based on the criteria described by Allen et al. (2004): Class I sources are protostars with interstellar envelopes and Class II sources are disk-dominated objects. However, background galaxies and evolved stars such as asymptotic giant branch (AGB) stars can also be red sources. In order to make a more pure YSO candidate sample, we removed star-formation (PAH)
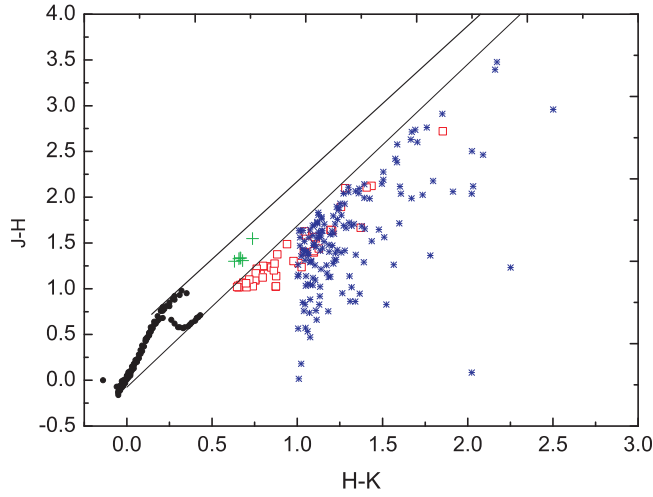
Fig. 3 Color-Color diagram of the 2MASS YSO candidates projected on to Sh2-82. The P_1, P_{1+} and P_2 sources are indicated by red boxes, green pluses and blue asterisks, respectively.
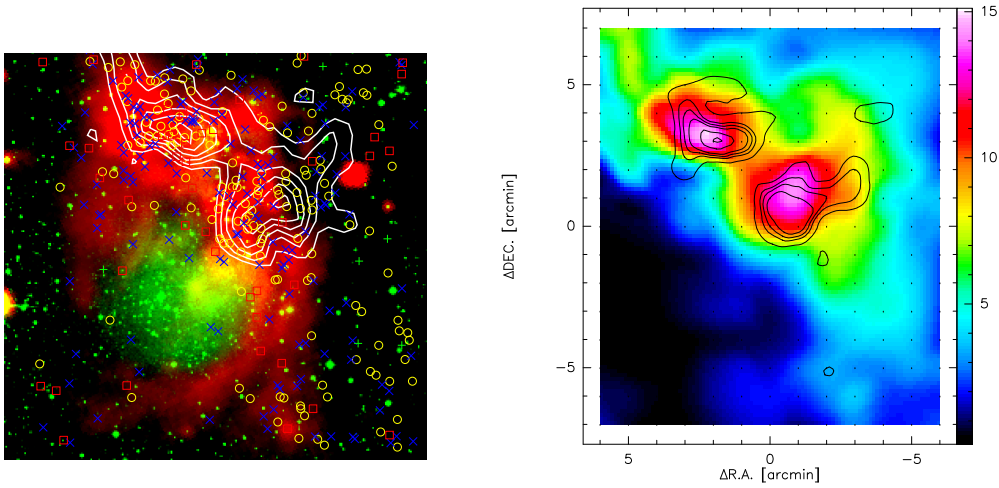

Fig. 4 Two young clusters found through the 2MASS point catalog. *Left*: P_1, P_{1+}, P_2 and P_3 sources, indicated by red boxes, green pluses, blue crosses and yellow circles, respectively. The contour levels are the same as Fig. 1 for the $^{13}CO(J = 1–0)$ emission. *Right*: contours corresponding to stellar density ranges of 5, 7, 8, 10 and 12 $arcmin^{-2}$ superimposed onto the emission intensity of ^{13}CO (1–0).

galaxies and weak-line AGNs via a series of cuts in the four-band IRAC color-color diagrams using the procedure developed by Gutermuth et al. (2008). The color criteria for both AGB stars and extragalactic contaminants from Harvey et al. (2006) were also used to filter our sample.

Figure 5 (right image) shows the final distributions of both the Class I (magenta pluses) and Class II (cyan pluses) point sources around Sh2-82. It can be noted that most YSOs prefer to be located
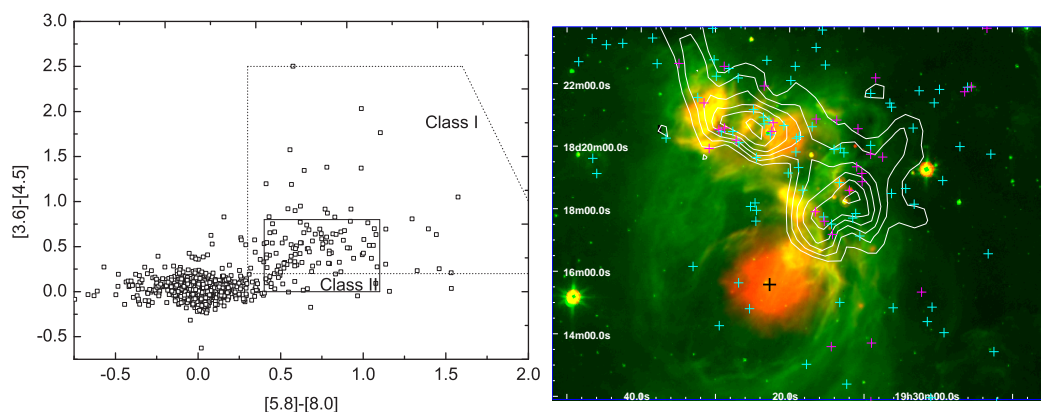
Fig. 5 *Left*: the distribution of YSOs within the color selection criteria of Allen et al. (2004). *Right*: a two-color image of Sh2-82: 8 μm emission (*green*) and 24 μm emission (*red*). The magenta pluses are Class I and the cyan pluses are Class II YSOs. The black plus is the ionizing star of this H II region.
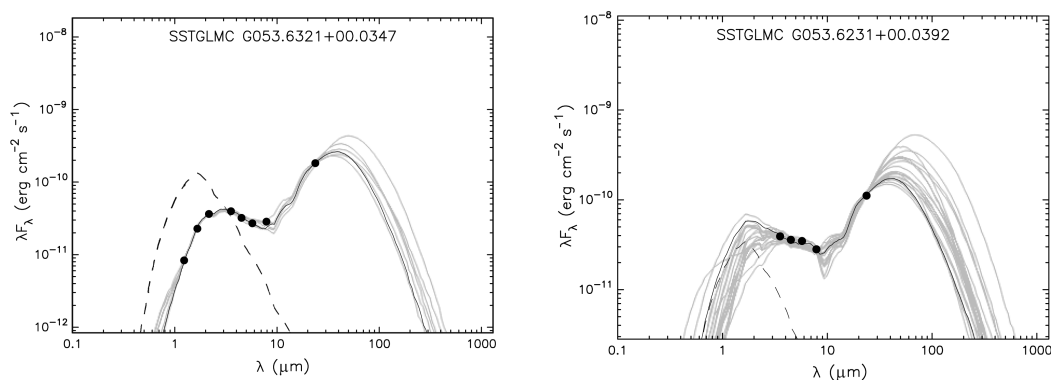

Fig. 6 Two examples of the SED fitting model. The dashed line represents the stellar photosphere model. The black line represents the best-fitting SED, and the gray lines represent all the other acceptable YSO fits.

on the northwest corner of Sh2-82, and nearly all Class I sources are projected onto the molecular clumps. Since molecular clouds are birth places of stars, we expect some of these sources to be YSOs whose formation could have been triggered by the expansion of Sh2-82. We also perform a fitting of these YSO candidates in the IRAC and 2MASS bands to derive their spectral energy distribution (SED). We limit our study to the sources superimposed on the two molecular clumps. Briefly, the SED fitting tool works as a regression method to find the SEDs within a specified χ^2 from a large grid of models after fitting the input data points. The grid of models contains stellar masses, disk masses, mass accretion rates and line-of-sight (LOS) inclinations. The grid of the YSO models was computed by Robitaille et al. (2006) using the 20 000 two-dimensional radiation transfer models from Whitney et al. (2003a,b, 2004). Each YSO model has SEDs for 10 viewing angles (inclinations), so the total YSO grid consists of 200 000 SEDs. Observations from the J-band to 24 μm are fitted using a χ^2-

Table 1 Parameters derived from the SED fitting of sources projected onto the molecular clumps.

Source Name	R. A. (J2000)	Dec (J2000)	M ($M_\odot$)	χ^2 (total)	M_{disk} ($M_\odot$)	$\dot{M}_{\mathrm{env}}$ ($M_\odot\,\mathrm{yr}^{-1}$)
SSTGLMC G053.6168+00.0448	292.5866	18.34431	3.72	5.65	2.15×10^{-4}	0.00
SSTGLMC G053.6209+00.0406	292.5926	18.34584	1.82	5.04	6.52×10^{-3}	9.96×10^{-6}
SSTGLMC G053.6172+00.0377	292.5934	18.34121	7.49	18	4.52×10^{-2}	5.56×10^{-5}
SSTGLMC G053.6160+00.0361	292.5942	18.33941	7.29	17.65	1.24×10^{-2}	3.04×10^{-5}
SSTGLMC G053.6231+00.0392	292.595	18.34714	2.21	2.6	9.16×10^{-2}	4.49×10^{-6}
SSTGLMC G053.6180+00.0352	292.596	18.34073	4.89	16.52	7.06×10^{-2}	1.32×10^{-4}
SSTGLMC G053.6404+00.0458	292.5976	18.36544	1.22	0.5	9.16×10^{-4}	9.01×10^{-6}
SSTGLMC G053.6227+00.0360	292.5977	18.34522	4.56	3.35	7.01×10^{-4}	2.21×10^{-5}
SSTGLMC G053.6260+00.0374	292.5981	18.34881	1.22	8.03	1.25×10^{-2}	1.1×10^{-5}
SSTGLMC G053.6089+00.0238	292.602	18.32729	3.36	5.58	1.28×10^{-3}	1.06×10^{-5}
SSTGLMC G053.6321+00.0347	292.6036	18.35283	3.37	11.8	2.38×10^{-3}	8.12×10^{-6}
SSTGLMC G053.6508+00.0357	292.6122	18.36969	1.41	9.20	6.95×10^{-4}	1.86×10^{-5}
SSTGLMC G053.6222+00.0188	292.6134	18.33653	3.84	6.19	5.68×10^{-4}	9.85×10^{-6}
SSTGLMC G053.6272+00.0194	292.6153	18.34119	4.63	13.93	1.10×10^{-3}	1.43×10^{-7}
SSTGLMC G053.6576+00.0337	292.6175	18.37475	3.15	3.61	2.76×10^{-6}	0.00
SSTGLMC G053.6309+00.0165	292.6199	18.34309	5.43	9.91	4.47×10^{-4}	4.15×10^{-4}
SSTGLMC G053.6300+00.0140	292.6217	18.34109	2.92	6.00	6.80×10^{-2}	1.24×10^{-6}
SSTGLMC G053.6316+00.0134	292.6231	18.34215	0.17	3.56	1.81×10^{-2}	4.73×10^{-6}
SSTGLMC G053.6572+00.0259	292.6245	18.37064	1.77	3.12	6.33×10^{-3}	1.46×10^{-6}
SSTGLMC G053.6654+00.0291	292.6258	18.37940	1.32	5.81	3.84×10^{-4}	7.25×10^{-8}
SSTGLMC G053.6253+00.0040	292.6285	18.33213	0.34	0.6	1.72×10^{-4}	5.60×10^{-6}
SSTGLMC G053.6479+00.0133	292.6314	18.35639	5.3	6.99	3.08×10^{-2}	3.46×10^{-4}
SSTGLMC G053.6520+00.0118	292.6349	18.35930	1.87	1.49	1.69×10^{-2}	2.76×10^{-5}
SSTGLMC G053.6411-00.0133	292.6527	18.33765	1.83	8.47	1.38×10^{-3}	5.63×10^{-5}
SSTGLMC G053.5813+00.0781	292.5379	18.32906	3.43	0.57	1.18×10^{-3}	0.00
SSTGLMC G053.5854+00.0803	292.5379	18.33374	0.27	1.12	2.89×10^{-3}	5.78×10^{-6}
SSTGLMC G053.5706+00.0670	292.5427	18.31441	1.2	2.63	9.84×10^{-2}	1.31×10^{-5}
SSTGLMC G053.5745+00.0690	292.5428	18.31878	0.52	3.13	2.70×10^{-3}	3.86×10^{-6}
SSTGLMC G053.5790+00.0683	292.5457	18.32236	0.13	0.48	1.50×10^{-4}	8.59×10^{-7}
SSTGLMC G053.5573+00.0559	292.5463	18.29744	1.31	5.07	4.79×10^{-2}	1.79×10^{-6}
SSTGLMC G053.5560+00.0533	292.548	18.29500	2.09	9.22	2.261×10^{-3}	5.19×10^{-6}
SSTGLMC G053.5888+00.0659	292.5529	18.32982	2.01	0.84	2.88×10^{-2}	7.35×10^{-4}
SSTGLMC G053.5918+00.0654	292.5549	18.33224	2.16	2.85	5.10×10^{-4}	2.73×10^{-5}
SSTGLMC G053.5760+00.0562	292.5554	18.31393	6.5	28	2.56×10^{-6}	0.00
SSTGLMC G053.5928+00.0622	292.5584	18.33156	2.49	2.43	1.33×10^{-2}	8.37×10^{-6}
SSTGLMC G053.5535+00.0397	292.5593	18.28632	2.95	1.51	4.21×10^{-3}	0.00
SSTGLMC G053.5586+00.0419	292.5599	18.29182	3.21	2.00	1.45×10^{-1}	1.13×10^{-4}
SSTGLMC G053.5640+00.0400	292.5643	18.29563	5.63	0.23	3.60×10^{-2}	7.73×10^{-5}
SSTGLMC G053.5685+00.0375	292.5689	18.29842	5.65	2.23	2.62×10^{-3}	1.25×10^{-5}
SSTGLMC G053.6090+00.0578	292.5707	18.34370	0.28	1.32	6.74×10^{-4}	5.05×10^{-6}
SSTGLMC G053.5818+00.0372	292.5759	18.30991	3.34	8.59	2.34×10^{-3}	2.55×10^{-5}
SSTGLMC G053.6078+00.0492	292.578	18.33848	1.03	5.36	2.11×10^{-4}	6.46×10^{-6}
SSTGLMC G053.5935+00.0409	292.5784	18.32195	2.69	4.17	1.73×10^{-2}	4.65×10^{-5}
SSTGLMC G053.6077+00.0474	292.5796	18.33759	0.42	2.27	2.05×10^{-2}	1.93×10^{-4}
SSTGLMC G053.6014+00.0437	292.5799	18.33025	4.96	9.44	7.44×10^{-5}	5.05×10^{-6}
SSTGLMC G053.5935+00.0347	292.5841	18.31903	4.02	16.71	6.17×10^{-3}	3.40×10^{-8}

minimization technique. We consider sources with $\chi^2/N_{\mathrm{data}} < 4$ to be well fitted. Our results are listed in Table 1.

Figure 6 shows two examples of the SED fitting results. From these fits, we can see that there is a large infrared excess, which is inferred to be a planetary disk around the central stars (Wang & Hu
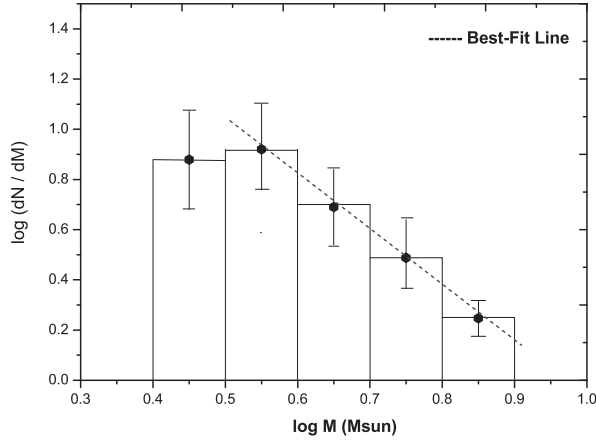
Fig. 7 Mass distribution function for YSOs in Sh2-82. The error bars represent $\pm \sqrt{N}$ errors.

1994). None of the selected YSO candidates were better fitted by a pure stellar photosphere model, confirming our YSO color selection criteria for this region.

If we assume the following form of a mass function

$$\frac{dN}{dM} = A(M/M_\odot)^{-\Gamma},$$ (3)

then the distribution of the masses of YSOs in Sh2-82 can be estimated. By studying M17, Povich et al. (2009) found that the GLIMPSE Point Source Archive essentially recovers all YSOs above $\sim$ 3 $M_\odot$ toward those regions. As is also apparent in Figure 7, the deviation from a single power law becomes progressively worse in the lower mass bin. Using the highest four mass bins (from 3.16 $M_\odot$ to 8 $M_\odot$) yields a slope of $\Gamma = 2.21 \pm 0.45$, which is approximately consistent with the classical value of 2.35 derived by Salpeter (1955) for the mass range $0.4 < M/M_\odot \leq 10$.

3 DISCUSSION

Although Sh2-82 is seen at the edge of the pulsar wind nebula (PWN) G54.1+0.3, it is not related to the PWN, the center of which has a distance of at least 5 kpc (Weisberg et al. 2008). G54.1+0.3 is likely to be at a distance of $\approx$ 6.2 kpc due to the morphological association of the PWN with a CO molecular cloud at a velocity of ≈ 53 km s^{-1}, as revealed by high-resolution ^{13}CO images (Leahy et al. 2008). We now discuss the likelihood of triggering star formation in Sh2-82. According to the model of Elmegreen & Lada (1977), a thin layer of compressed neutral material forms between a shock front and a slow-moving D-type ionization front. This may be the configuration observed in Sh2-82. In the triggering star-formation scenario, the ages of the ionizing star(s) must be older than the ages of the second generation stars plus the shock front traveling time. However, a problem with Elmegreen & Lada's model concerns the ages and sizes of the H II regions.

Using the model described by Dyson & Williams (1980), we calculate the dynamical age of the H II region at a given radius R as

$$t(R) = \frac{4R_{\rm s}}{7c_{\rm s}} \left[\left(\frac{R}{R_{\rm s}} \right)^{7/4} - 1 \right],$$ (4)

where $c_{\rm s}$ is the sound velocity in the ionized gas ($c_{\rm s} = 10$ km s^{-1}) and $R_{\rm s}$ is the radius of the Strömgren sphere given by $R_{\rm s} = (3N_{uv}/4\pi n_0^2 \alpha_B)^{1/3}$, where N_{uv} represents the Lyman continuum

photons emitted by the ionizing star per second, and $\alpha_B = 2.6 \times 10^{-13}$ cm^3 s^{-1} is the hydrogen recombination coefficient. Sh2-82 is excited by a B0V star, which emits 1.25×10^{48} ionizing photons per second (Vacca et al. 1996; Schaerer & de Koter 1997). The present radius of Sh2-82 could be calculated to be 2.2 ± 0.5 pc at a distance of 1.7 ± 0.4 kpc. We derived a dynamical age of between 0.25 and 0.48 Myr, assuming an original ambient density of $(1 \pm 0.5) \times 10^3$cm^{-3}.

Whitworth et al. (1994, hereafter W94) presented an analytical treatment of the collect-and-collapse process. A shock front forms and gathers material until it is able to fragment and collapse to form stars. The fragmentation time and radius can be calculated as

$$t_{\text{frag}} = 1.56 \text{ Myr} \times a_{0.2}^{7/11} L_{49}^{-1/11} n_3^{-5/11}, \tag{5}$$

$$R_{\text{frag}} = 5.8 \text{ pc} \times a_{0.2}^{4/11} L_{49}^{1/11} n_3^{-6/11}, \tag{6}$$

where $a_{0.2}$ is the sound speed inside the shocked layer in units of 0.2 km s^{-1}, L_{49} is the central source's ionizing flux in units of 10^{49} photons s^{-1}, and n_3 is the initial gas number density in units of 10^3cm^{-3}. Since we cannot calculate an appropriate value for $a_{0.2}$ from our current data sets, we adopt a value of 1.0 as Koenig et al. (2008) did in the analysis of W5. We find that the fragmentation process in the periphery of Sh2-82 should occur between 1.6 and 5.3 Myr after its formation, a later point in time than its dynamical age derived above. We thus discard the so-called collect and collapse as being the mechanism responsible for YSO formation. Other processes such as radiative-driven implosions and/or collisions with pre-existing molecular core(s) may operate; we can see from Figure 1 that the CO emission overlaps the densest part of the MSXA shell, which may be evidence of the radiation driving this process. Sh2-82 is not the only object; H II regions like Sh2-235 (Kirsanova et al. 2008), Sh2-217 and Sh2-219 (Deharveng et al. 2003) also show such physical processes of sequential star formation.

4 SUMMARY

The interstellar medium and its young stellar objects around the H II region Sh2-82 have been analyzed. Two molecular clumps were found from the archived data of GRS. We found two young corresponding clusters with 2MASS data embedded in the two molecular clumps. By using an SED fitting to each of the YSO candidates with infrared excess, we derived the mass function slopes in this region. Comparing the H II region's dynamical age and the fragmentation time of the molecular shell, we discarded the so-called collect and collapse as being the triggering process for YSO formation. Sh2-82 can be a mixture of other processes such as radiative-driven implosion and/or collisions with pre-existing clumps. More numerical studies and deeper observations should be carried out in the future to reveal an even clearer picture of triggered star formation in H II regions.

References

Allen, L. E., Calvet, N., D'Alessio, P., et al. 2004, ApJS, 154, 363

Benjamin, R. A., Churchwell, E., Babler, B. L., et al. 2003, PASP, 115, 953

Bertoldi, F., & McKee, C. F. 1990, ApJ, 354, 529

Brand, J., & Blitz, L. 1993, A&A, 275, 67

Carey, S. J., Noriega-Crespo, A., Price, S. D., et al. 2005, in American Astronomical Society Meeting Abstracts, Bulletin of the American Astronomical Society, 37, 1252

Deharveng, L., Zavagno, A., Salas, L., et al. 2003, A&A, 399, 1135

Dyson, J. E., & Williams, D. A. 1980, Physics of the Interstellar Medium (Manchester: Manchester Univ. Press)

Elmegreen, B. G., & Lada, C. J. 1977, ApJ, 214, 725

Fazio, G. G., Hora, J. L., Allen, L. E., et al. 2004, ApJS, 154, 10

Gutermuth, R. A., Myers, P. C., Megeath, S. T., et al. 2008, ApJ, 674, 336

Harvey, P. M., Chapman, N., Lai, S.-P., et al. 2006, ApJ, 644, 307

Hester, J. J., Desch, S. J., Healy, K. R., & Leshin, L. A. 2004, Science, 304, 1116

Hunter, D. A., & Massey, P. 1990, AJ, 99, 846

Jackson, J. M., Rathborne, J. M., Shah, R. Y., et al. 2006, ApJS, 163, 145

Kerton, C. R., Arvidsson, K., Knee, L. B. G., & Brunt, C. 2008, MNRAS, 385, 995

Kirsanova, M. S., Sobolev, A. M., Thomasson, M., et al. 2008, MNRAS, 388, 729

Koenig, X. P., Allen, L. E., Gutermuth, R. A., et al. 2008, ApJ, 688, 1142

Lahulla, J. F. 1985, A&AS, 61, 537

Leahy, D. A., Tian, W., & Wang, Q. D. 2008, AJ, 136, 1477

Lefloch, B., & Lazareff, B. 1994, A&A, 289, 559

Miao, J., White, G. J., Nelson, R., Thompson, M., & Morgan, L. 2006, MNRAS, 369, 143

Miao, J., White, G. J., Thompson, M. A., & Nelson, R. P. 2009, ApJ, 692, 382

Povich, M. S., Churchwell, E., Bieging, J. H., et al. 2009, ApJ, 696, 1278

Rieke, G. H., & Lebofsky, M. J. 1985, ApJ, 288, 618

Rieke, G. H., Young, E. T., Engelbracht, C. W., et al. 2004, ApJS, 154, 25

Robitaille, T. P., Whitney, B. A., Indebetouw, R., Wood, K., & Denzmore, P. 2006, ApJS, 167, 256

Salpeter, E. E. 1955, ApJ, 121, 161

Schaerer, D., & de Koter, A. 1997, A&A, 322, 598

Skrutskie, M. F., Cutri, R. M., Stiening, R., et al. 2006, AJ, 131, 1163

Vacca, W. D., Garmany, C. D., & Shull, J. M. 1996, ApJ, 460, 914

Wang, J.-J., & Hu, J.-Y. 1994, Chinese Astronomy and Astrophysics, 18, 67

Weisberg, J. M., Stanimirović, S., Xilouris, K., et al. 2008, ApJ, 674, 286

Whitney, B. A., Wood, K., Bjorkman, J. E., & Cohen, M. 2003a, ApJ, 598, 1079

Whitney, B. A., Wood, K., Bjorkman, J. E., & Wolff, M. J. 2003b, ApJ, 591, 1049

Whitney, B. A., Indebetouw, R., Bjorkman, J. E., & Wood, K. 2004, ApJ, 617, 1177

Whitworth, A. P., Bhattal, A. S., Chapman, S. J., Disney, M. J., & Turner, J. A. 1994, MNRAS, 268, 291

Wilson, T. L., & Rood, R. 1994, ARA&A, 32, 191